Received: 22 June 2023 | Revised: 21 July 2023 | Accepted: 23 August 2023

DOI: 10.1002/pamm.202300032

RESEARCH ARTICLE

A material model for thick, rate-dependent adhesives with delocalized softening

Aaron Schumacher | **Anton Matzenmiller**

Department of Mechanical Engineering, Institute of Mechanics, University of Kassel, Kassel, Germany

Correspondence
Anton Matzenmiller, Department of Mechanical Engineering, Institute of Mechanics, University of Kassel, Mönchebergstr. 7, 34125 Kassel, Germany.
Email: amat@uni-kassel.de

Abstract

This contribution is dedicated to the development and implementation of a material model to describe the deformation behaviour of assembly adhesives. These assembly adhesives are usually used with thicknesses of several millimetres up to centimetres in order to compensate for large relative displacements of joining parts. These large displacements can be resisted by assembly adhesives, since they have a low shear modulus and thus a high strain until failure above their glass transition temperature. As a basis, the isothermal and isotropic hyperelasticity theory is used to describe the elastic deformation behaviour up to the postcritical range by using an isochoric–volumetric decomposition of the deformation gradient. The ARRUDA–BOYCE and OGDEN models are employed here for the isochoric-elastic and volumetric-elastic description. The modelling of the rate-dependence concerning shear and bulk viscosity succeeds by extending the hyperelasticity theory to the theory of finite viscoelasticity with the generalized MAXWELL model in each case. In order to model the postcritical deformation behaviour, an isotropic damage model is developed based on the energy limiting method and used to define an isochoric and a volumetric damage variable, so that the mapping of softening due to change of shape, as well as cavitation, succeeds. Furthermore, the damage variables are delocalized to prevent pathological mesh dependence by using the integral regularization method. Finally, the material parameters are determined and validated by means of measurement data due to tests at the assembly adhesive BETAFORCE 2850L. The results demonstrate a high prediction quality.

1 | INTRODUCTION

In comparison to other materials, the description of the deformation behaviour of cold-curing assembly adhesives, based on polyurethane, is not too advanced. According to the measurement data, assembly adhesives react with viscoelastic and temperature-dependent deformations to loads above their glass transition temperature. Finally, they undergo a softening behaviour above a material-specific energy density, see Figures 1–4. Consequently, the hyperelasticity theory is used as a

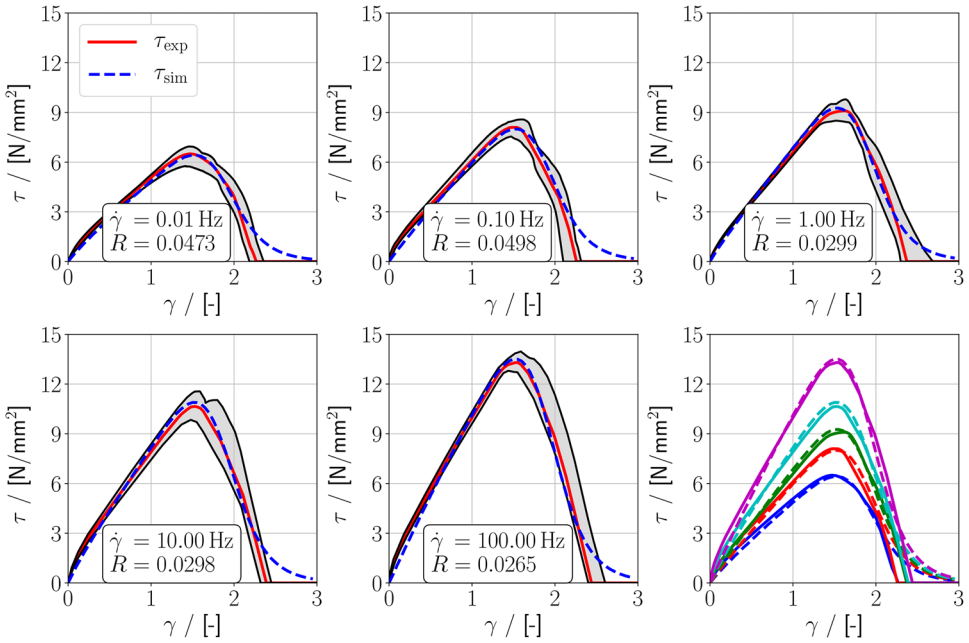

FIGURE 1 Verification results on the shear specimen with an adhesive layer thickness of 2 mm.

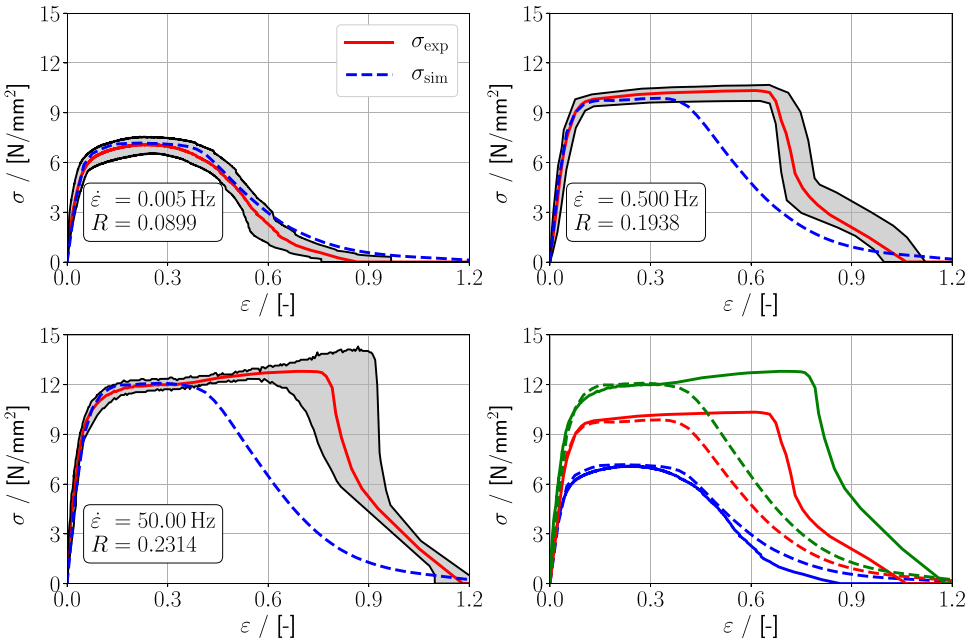

FIGURE 2 Verification results on the butt joint specimen with an adhesive layer thickness of 2 mm.

basis for the description of the elastic deformation behaviour, see [1].

$$\boldsymbol{\sigma} : \mathbf{d} - \dot{\Psi}_t \geq 0. \tag{1}$$

In Equation (1) $\boldsymbol{\sigma}$, $\mathbf{d}$ and Ψ_t denote the CAUCHY stress tensor, the rate of deformation tensor and the HELMHOLTZ free energy, respectively. Notice that the assumption of temperature independence has been included in Equation (1), which will be assumed in the course of this work. As further assumptions, the homogeneity, isotropy and representation in the form of invariants are also adopted within the scope of this work, see [2] and [3].

For further capturing of the rate-dependence and the softening behaviour, the hyperelasticity theory is extended to the theory of finite viscoelasticity, see [4], and then enhanced by a suitable delocalized damage model. Since the volumetric

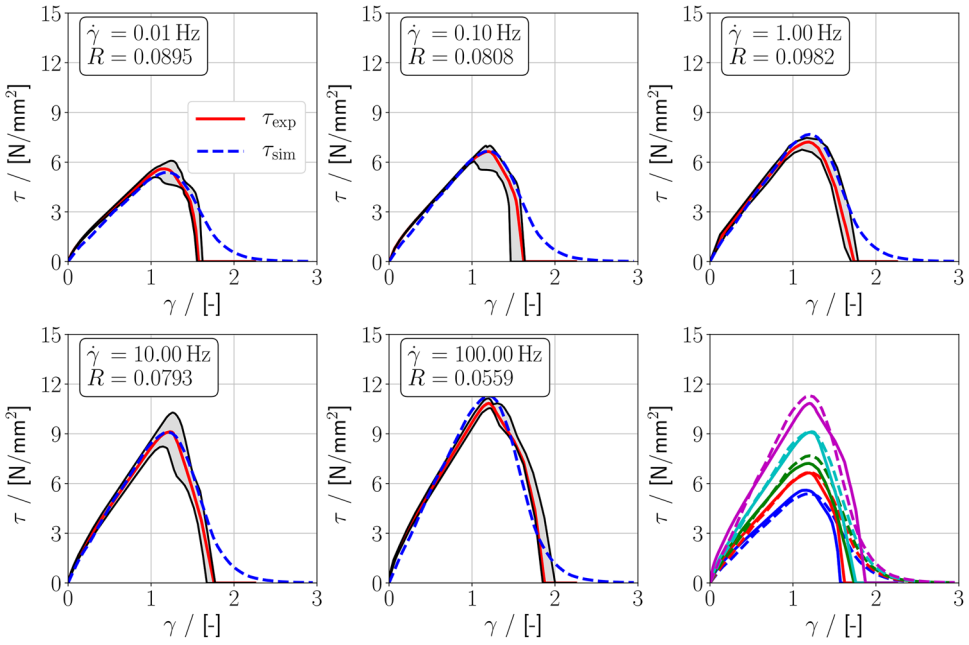

FIGURE 3 Validation results on the shear specimen with an adhesive layer thickness of 5 mm.

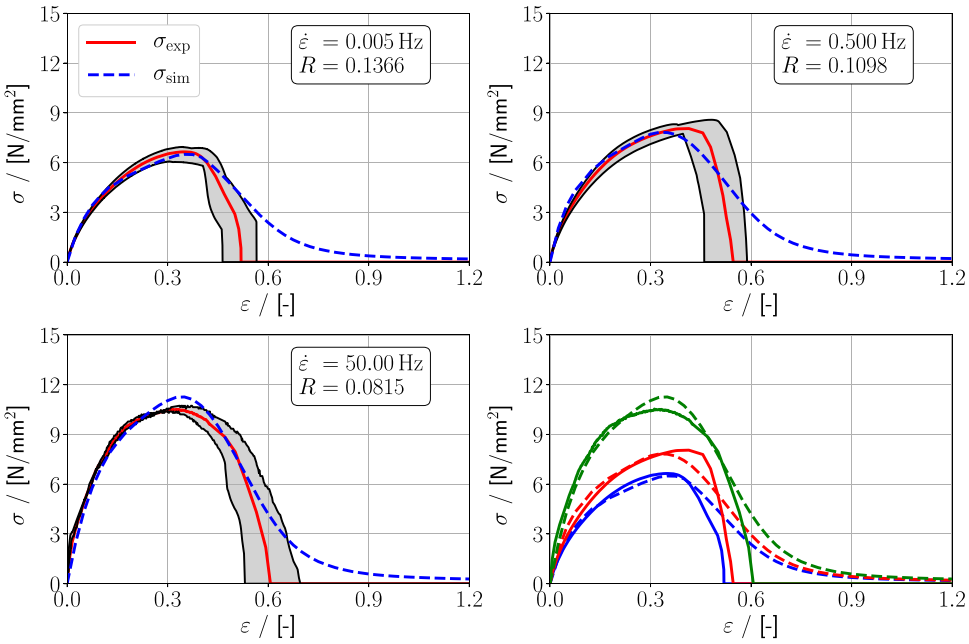

FIGURE 4 Validation results on the butt joint specimen with an adhesive layer thickness of 5 mm.

and isochoric deformation behaviour of assembly adhesives has to be differentiated, the separate description of the volumetric and isochoric parts of the elasticity, viscosity and softening is enabled by a volumetric–isochoric decomposition of the deformation gradient, see [5]. Altogether, this results in an additive description of the HELMHOLTZ free energy, consisting of a total of six different energy density functions, see [6].

$$\Psi_{\mathrm{t}}^{\mathrm{d}} = \Psi_{\mathrm{vol}}^{\mathrm{d}}\left(\Psi_{\mathrm{vol}}^{\mathrm{eq}}\right) + \Psi_{\mathrm{iso}}^{\mathrm{d}}\left(\Psi_{\mathrm{iso}}^{\mathrm{eq}}\right) + \sum_{i=1}^{n_{\mathrm{vol}}} \Upsilon_{\mathrm{vol},i}^{\mathrm{ov}} + \sum_{i=1}^{n_{\mathrm{iso}}} \Upsilon_{\mathrm{iso},i}^{\mathrm{ov}}. \tag{2}$$

In Equation (2), the energy functions $\Psi_{\mathrm{vol}}^{\mathrm{eq}}$ and $\Psi_{\mathrm{iso}}^{\mathrm{eq}}$ as well as $\Upsilon_{\mathrm{vol},i}^{\mathrm{ov}}$ and $\Upsilon_{\mathrm{iso},i}^{\mathrm{ov}}$ describe the viscoelastic deformation behaviour. In addition, $\Psi_{\mathrm{vol}}^{\mathrm{d}}$ and $\Psi_{\mathrm{iso}}^{\mathrm{d}}$ denote limiters for the maximum energy density that a material can withstand.

By inserting the material rate of the HELMHOLTZ free energy into Equation (1) and applying the COLEMAN–NOLL procedure, the stress calculation may be further derived, see [7]. Notice that the additive description by six parts is inherited to the CAUCHY stress tensor.

$$\boldsymbol{\sigma}^{\mathrm{d}} = \frac{d\widetilde{\Psi^{\mathrm{d}}_{\mathrm{vol}}}}{d\Psi^{\mathrm{eq}}_{\mathrm{vol}}}\boldsymbol{\sigma}^{\mathrm{eq}}_{\mathrm{vol}} + \frac{d\widetilde{\Psi^{\mathrm{d}}_{\mathrm{iso}}}}{d\Psi^{\mathrm{eq}}_{\mathrm{iso}}}\boldsymbol{\sigma}^{\mathrm{eq}}_{\mathrm{iso}} + \boldsymbol{\sigma}^{\mathrm{ov}}_{\mathrm{vol}} + \boldsymbol{\sigma}^{\mathrm{ov}}_{\mathrm{iso}} \qquad \text{with} \qquad \frac{d\widetilde{\Psi^{\mathrm{d}}}}{d\Psi^{\mathrm{eq}}} = 1 - \widetilde{D}. \tag{3}$$

Again, in Equation (3) $\boldsymbol{\sigma}^{\mathrm{eq}}_{\mathrm{vol}}$ and $\boldsymbol{\sigma}^{\mathrm{eq}}_{\mathrm{iso}}$ describe the elastic parts of the CAUCHY stress tensor. Furthermore, $\boldsymbol{\sigma}^{\mathrm{ov}}_{\mathrm{vol}}$ and $\boldsymbol{\sigma}^{\mathrm{ov}}_{\mathrm{iso}}$ represent the sum of the viscous parts of the CAUCHY stress tensor. The volumetric and isochoric multipliers in front of the elastic parts of the CAUCHY stress tensor in Equation (3) result due to the limiters for the maximum energy density in Equation (2). These multipliers are related to delocalized, scalar damage variables $\widetilde{D}$ of continuum damage mechanics, see [8].

2 | MATERIAL MODEL

The volumetric-elastic part of the HELMHOLTZ free energy is described by the volumetric model of OGDEN, containing two material parameters: The bulk modulus K, where $K \in \mathbb{R}^{+}_{\neq 0}$, and a parameter β, where $\beta \in \mathbb{R}^{-} \setminus [-1, 0]$, enabling a modification concerning softer and stiffer deformation behaviour for larger strains, see [9].

$$\Psi^{\mathrm{eq}}_{\mathrm{vol}} = \frac{K}{\beta^2}\left(III_{\mathrm{F}}^{-\beta} - 1 + \beta \ln(III_{\mathrm{F}})\right). \tag{4}$$

For the description of the isochoric-elastic part of the HELMHOLTZ free energy, the isochoric model of ARRUDA–BOYCE with two material parameters is employed: The shear modulus G, where $G \in \mathbb{R}^{+}_{\neq 0}$, and a parameter N, where $N \in \mathbb{R}^{+}_{\neq 0}$, describing the polymer chain length and, thus, a stiffening deformation behaviour with increasing strains, see [10].

$$\Psi^{\mathrm{eq}}_{\mathrm{iso}} = GN \sum_{i=1}^{20} b_i \frac{I^{i}_{\mathrm{b,iso}} - 3^i}{N^i} \qquad \text{with} \qquad b_i = \left\{ \frac{1}{2}, \frac{1}{20}, \left\{ \exp\left(-\frac{12466i + 8471}{10000} \right) \middle| \; i \geq 3 \right\} \right\}. \tag{5}$$

The modelling of rate-dependence concerning bulk and shear viscosity succeeds by introducing inner variables $\mathbf{q}_{\mathrm{vol},i}$ and $\mathbf{q}_{\mathrm{iso},i}$ and employing the generalized MAXWELL model, which has two material parameters for each MAXWELL-chain: The factors of involvement γ_i, where $\gamma_i \in [0, 1]$, and the relaxation times τ_i, where $\tau_i \in \mathbb{R}^{+}_{\neq 0}$, see [11]. According to the measurement data, five isochoric and three volumetric MAXWELL-chains are defined to describe the viscoelastic spectra, see Figures 1 and 2.

$$\dot{\mathbf{q}}_i + \frac{1}{\tau_i}\mathbf{q}_i = \frac{\gamma_i}{\tau_i}\boldsymbol{\sigma}^{\mathrm{eq}} \qquad \text{with} \qquad \lim_{t \to -\infty} \mathbf{q}_i = \mathbf{0}. \tag{6}$$

The description of the postcritical deformation behaviour is realized by employing the energy limiting method in each case. This method, proposed by VOLOKH, offers a convenient way to enhance viscoelastic material models to strain softening and, therefore, the prediction of damage, see [12]. As limiting potentials $\Psi^{\mathrm{d}}_{\mathrm{vol}}$ and $\Psi^{\mathrm{d}}_{\mathrm{iso}}$ with three parameters each Φ_0, n and α, where $\Phi_0 \in \mathbb{R}^{+}_{\neq 0}$, $n \in \mathbb{R}^{+}_{\neq 0}$ and $\alpha \in [0, 1]$, the new proposal $\Psi^{\mathrm{d}}_{\mathrm{IFM}}$ in Equation (7) is used to define an isochoric and a volumetric softening multiplier, see [8].

$$\Psi^{\mathrm{d}}_{\mathrm{IFM}} = \Phi_0 \frac{\Psi_{\mathrm{m}}}{\sqrt[n]{1 + \Psi^{n}_{\mathrm{m}}}} \qquad \text{with} \qquad \Psi_{\mathrm{m}} = (1 - \alpha)\frac{\Psi^{\mathrm{eq}}}{\Phi_0} + \alpha \ln\left(1 + \frac{\Psi^{\mathrm{eq}}}{\Phi_0}\right). \tag{7}$$

The initial energy limiting method models reversible damage, which heals during unloading of a material. In order to transform the physically implausible modelling approach from reversible to irreversible damage, an additional internal variable has to be introduced, see [13]. In the scope of this work, the all-time maximum elastic energy $\Psi^{\mathrm{eq,max}}$ is proposed as a new variable.

$$\Psi^{\mathrm{eq,max}} = \max_{-\infty < s \leq t} \Psi^{\mathrm{eq}}. \tag{8}$$

TABLE 1 Identified and verified material parameters.

Deformation range	Volumetric parameters		Isochoric parameters	
Elasticity	K	$165\,\mathrm{N/mm^2}$	G	$10.8\,\mathrm{N/mm^2}$
	β	-2	N	19
Viscosity	$\gamma_{\mathrm{vol},\infty}$	0.61	$\gamma_{\mathrm{iso},\infty}$	0.34
	$\gamma_{\mathrm{vol},i}$	$\{0.09, 0.26, 0.04\}$	$\gamma_{\mathrm{iso},i}$	$\{0.24, 0.14, 0.05, 0.10, 0.13\}$
	$\tau_{\mathrm{vol},i}$	$\{0.005, 0.5, 50\}\,\mathrm{s}$	$\tau_{\mathrm{iso},i}$	$\{0.01, 0.1, 1, 10, 100\}\,\mathrm{s}$
Softening	$\Phi_{\mathrm{vol},0}$	$0.72\,\mathrm{N/mm^2}$	$\Phi_{\mathrm{iso},0}$	$22\,\mathrm{N/mm^2}$
	n_{vol}	0.8	n_{iso}	4.5
	α_{vol}	0	α_{iso}	0.03
Delocalizing	L_{vol}	0.75 mm	L_{iso}	0.75 mm

This all-time maximum elastic energy is then used for the calculation of the multipliers in front of the elastic parts of the CAUCHY stress tensor by means of Equation (3), instead of the elastic energy. Therefore, during unloading of a material, the multipliers remain constant at the highest damage value reached within the deformation process of the material.

Finally, the softening multipliers by means of Equation (3) are delocalized to prevent pathological mesh dependence. In both cases, the integral regularization method using a linear weighting function is employed for this purpose introducing the nonlocal length L, where $L \in \mathbb{R}^{+}_{\neq 0}$, see [14].

$$\frac{d\widetilde{\Psi^{\mathrm{d}}}}{d\Psi^{\mathrm{eq}}} = \frac{1}{W_0}\int_{\Omega}\left(1 - \frac{\|\vec{x}-\vec{y}\|}{L}\right)\frac{d\Psi^{\mathrm{d}}}{d\Psi^{\mathrm{eq}}}\mathrm{d}\Omega \qquad \text{with} \qquad W_0 = \int_{\Omega}\left(1 - \frac{\|\vec{x}-\vec{y}\|}{L}\right)d\Omega. \tag{9}$$

Consequently, the delocalized multipliers at the locations $\vec{x}$ result from the weighting of the multipliers at the locations $\vec{y}$ with the weighting function over the radially symmetric range Ω with a radius of L.

3 | SIMULATION

In order to estimate the capability of the material model for engineering applications, measurement data concerning engineering stress versus engineering strain curves, τ-γ and σ-ε, on the polyurethane-based assembly adhesive BETAFORCE 2850L are used to identify the constitutive parameters, see Table 1. The test set-ups considered here are the shear and butt joint specimens with adhesive layer thicknesses of 2 and 5 mm in each case, respectively, see [15]. Due to the shear strain rates $\dot{\gamma} = \{0.01, 0.1, 1, 10, 100\}\,\mathrm{Hz}$, the shear specimen is subjected to five different rates of deformation, see Figures 1 and 3. Likewise, three different strain rates, $\dot{\varepsilon} = \{0.005, 0.5, 50\}\,\mathrm{Hz}$, are applied to the butt joint specimen, see Figures 2 and 4.

Concerning the parameter identification, verification and validation, measurement data on the shear and butt joint specimens with adhesive layer thicknesses of 2 mm are used to identify and verify the parameters. The shear specimen is employed to identify the isochoric parameters, since it obeys a homogeneous, isochoric stress state up to material failure in a good approximation. Afterwards, the volumetric parameters are identified sequentially to the isochoric ones by using the butt joint specimen. In Equation (9), the nonlocal lengths are determined by comparing results of a finite-element software with calculations performed by a stand-alone solver allowing the kinematics of simple shear and hydrostatic pressure to be enforced.

As shown in Figure 1, the verification of the isochoric material parameters on the shear specimen with an adhesive layer thickness of 2 mm reveals a good quality. All simulated stress responses lie within the range of the measurement data for each deformation rate up to the complete failure of the adhesive layer. In addition, the qualitative view of the prediction quality is strengthened by the calculation of mean square errors R of the simulated and experimental stress responses. Here, it is to be observed that the errors from the measurement data for all considered deformation rates are consistently less than 5%.

On the basis of the verification of the volumetric material parameters on the butt joint specimen with an adhesive layer thickness of 2 mm in Figure 2, a fair prediction quality for the viscoelastic range of deformation may be observed in two

cases. Furthermore, the evolution of the stress plateaus and their corresponding ordinates are well predicted for all rates of deformation. As expected, however, the rate-dependent length of the stress plateaus cannot be mapped as a result of the rate-independent damage model that is applied, based on the energy limiting method as proposed. Only for the lowest strain rate of $\dot{\varepsilon} = 0.005\,\mathrm{Hz}$ the stress-strain curve with its stress plateau is well-modelled on its entire course. However, this behaviour has been provoked by identifying the parameters describing the volumetric softening only by using the measured data at this deformation rate. Due to the application of a rate-independent damage model, the calculation of the mean square errors R tends to evaluate the quantitative prediction quality poorly with values up to 24% in the softening range. However, with the exception of the rate-dependent length of the stress plateaus, the stress responses simulated show a high level of congruency with the experimental stresses in the monotonously growing range for all deformation rates. If the rate-dependent length of the stress plateaus needs to be predicted correctly, a rate-dependent volumetric damage model has to be used.

In a next step, the validation of the volumetric and isochoric material parameters is performed by using measurement data of the shear and butt joint specimens with adhesive layer thicknesses of 5 mm to demonstrate the extrapolation capability.

In Figure 3, the validation result on the shear specimen with an adhesive layer thickness of 5 mm can be observed. The simulated stress response predicts the measurement data for all deformation rates with a high prediction quality. The simulated stresses lie within the range of the measurement data for all deformation rates up to failure of the adhesive layer. Slightly larger deviations appear just before the complete failure of the specimens, as the damage of the specimens for an adhesive layer thickness of 5 mm develops more brittle compared to the specimens with an adhesive layer thickness of 2 mm.

However, this variation cannot be mapped. Consequently, the quantitative prediction quality shows mean square errors R of up to 10%, which is slightly worse than for the shear specimens with an adhesive layer thickness of 2 mm. In general, however, there is a good extrapolation capability concerning larger values for the adhesive layer thickness.

The validation on the butt joint specimen with an adhesive layer thickness of 5 mm in Figure 4 shows a lower prediction quality compared to the validation on the shear specimen in Figure 3, with mean square errors R of up to 14%. The prediction quality of the viscoelastic range of deformation is good for all deformation rates, although the stress maximum at the highest deformation rate is overestimated by the simulation. The mapping of the postcritical range of deformation is only partly successful for all deformation rates, since the simulated specimens fail more ductile than the experimental ones. Thus, the simulated

stresses are not continuously within the range of the measured values after reaching the stress maximum in the various cases. A possible reason for the overestimation of the postcritical deformation behaviour is found in the identification process of the volumetric, softening parameters, as these parameters were only identified by using the measurement data for the lowest deformation rate. However, these data show a more ductile softening behaviour, compared to higher deformation rates of the same test set-up. Thus, the inclusion of higher deformation rates in the identification process would result in volumetric parameters that model a more brittle failure. However, due to the rate-independent damage model, these measurement data cannot be used to identify the parameters without fundamental manipulation of the experimental data, as it would require modifying the lengths of the stress plateaus. In general, it should be positively emphasized that no stress plateaus are predicted.

In addition to the verification of the material parameters and the validation based on the experimental and simulated stress responses to different deformation rates on the specimens with adhesive layer thicknesses of 2 and 5 mm, the evolution of the volumetric and isochoric softening is observed as a process over time. In order to investigate the damage evolution, the cross-sectional area orthogonal to the direction of loading is observed at half the height of the butt joint specimen. In this area, the softening multipliers of the energy limiting method are selected and presented as contour plots.

In Figure 5, consistent with the experimental results, it can be observed that the butt joint specimen with an adhesive layer thickness of 2 mm fails by starting in the radial centre due to processing damage. This failure form progresses radially outwards as a process of time and corresponds to cavitation due to the propagation of a discrete crack from the centre to the outer circumference. With a positive offset in time, compared to the volumetric failure, the same behaviour due to the redistribution of tensile stress is also observable for failure due to the change of shape. This interaction of volumetric and isochoric failure progresses for engineering strains up to approximately $\varepsilon = 0.6$ and, thus, is crucial for the evolution of the stress plateaus on the butt joint specimen with an adhesive layer thickness of 2 mm. For larger strains of $\varepsilon > 0.6$, failure additionally develops as a result of a change of shape in the radial direction from the outside to the inside, since the primary supporting cross-sectional area increasingly evolves to a circular ring as the strain increases. The supporting part of the

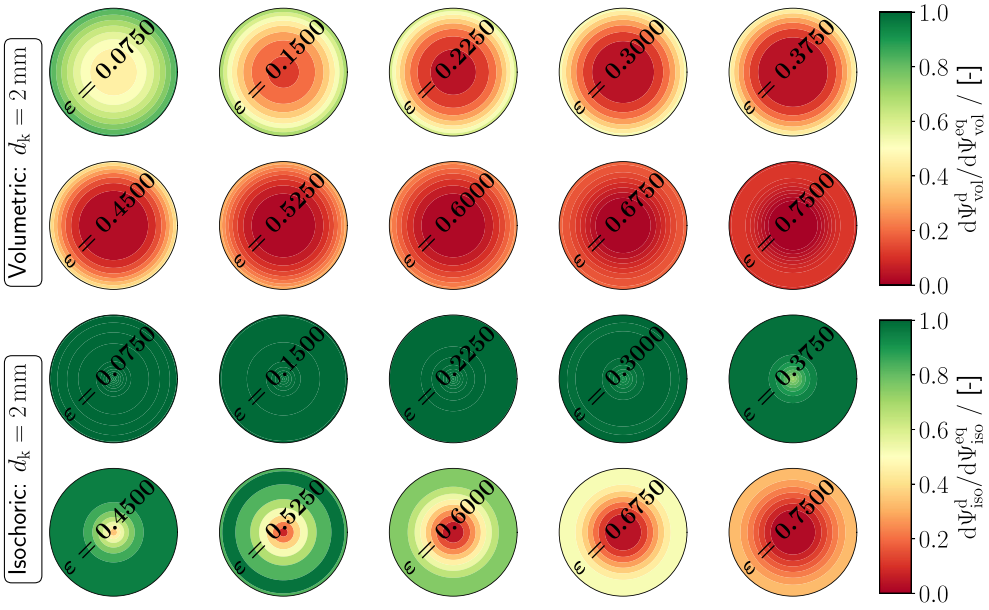

FIGURE 5 Softening on the butt joint specimen with an adhesive layer thickness of 2 mm.

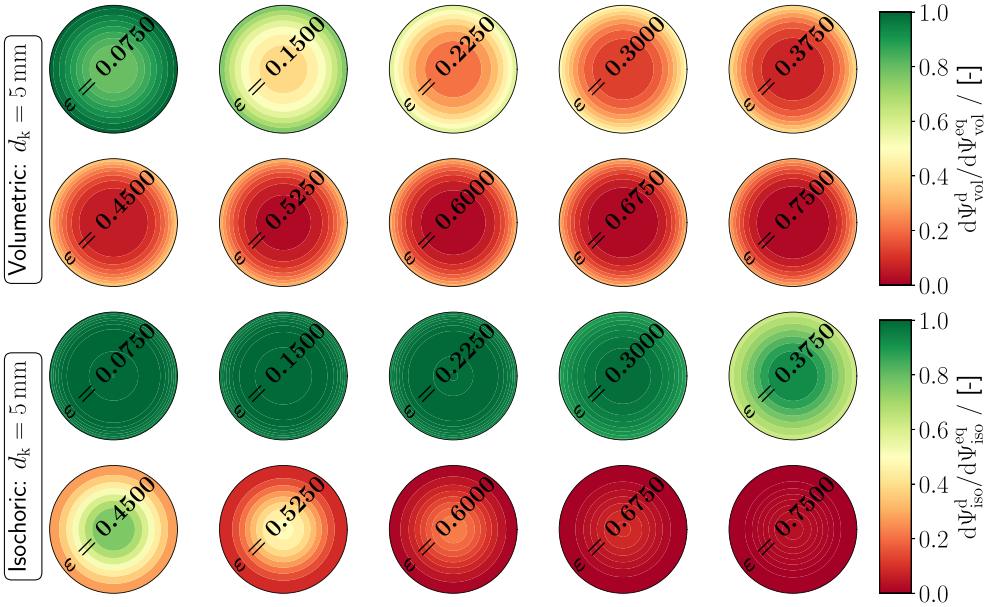

FIGURE 6 Softening on the butt joint specimen with an adhesive layer thickness of 5 mm.

entire specimen, hence increasingly corresponds to the geometry of a hollow cylinder, which itself has a significantly lower affinity to the formation of hydrostatic or transversal strain-restrained stress states compared to the initial, cylindrical geometry. Consequently, in the postcritical range of deformation, the ultimate load capacity of the butt joint specimen is dominated by the failure due to the change of shape, while the maximum load capacity and the stress plateaus result due to the interaction between a failure due to cavitation and change of shape.

Based on the illustration of the damage evolution over time in Figure 6, it is apparent that the simulated specimen for the butt joint with an adhesive layer thicknesses of 5 mm undergoes a different damage evolution than the former one. For the butt joint specimen with an adhesive layer thickness of 2 mm, the two softening multipliers evolve radially from the inside to the outside, with the isochoric damage showing a positive offset in time compared to the volumetric damage. In contrast, for the butt joint specimen with an adhesive layer thickness of 5 mm, it becomes apparent that the isochoric

softening multipliers develop from the outside to the inside in radial view. For larger strains of $\varepsilon > 0.3$, an additional, isochoric failure develops

in radial view from the inside to the outside. This failure mode results from the evolution of volumetric damage, which also develops in a radial view from the inside to the outside analogous to the butt joint specimen with an adhesive layer thickness of 2 mm. The inversion of the radial direction of isochoric damage appears to be crucial for the absence of distinct stress plateaus on the butt joint specimen with increasing adhesive layer thicknesses.

In Table 1, the identified material parameters are presented separately for the isochoric and volumetric ones. It is to be observed that all values for the material parameters lie within the range of expectations for assembly adhesives and, thus, are plausible.

4 | SUMMARY AND OUTLOOK

In the context of this work, a material model has been presented and verified that allows the description of the deformation behaviour of assembly adhesives up to complete failure of the material. In addition to capturing viscoelasticity based on theory of finite viscoelasticity, the material model contains two separate delocalized damage variables. These two isochoric and volumetric damage variables allow the modelling of failure modes corresponding to failure due to shape change and cavitation, respectively. On the one hand, by means of validation calculations, the extrapolation capacity of the material model has been shown with regard to varying adhesive layer thicknesses. On the other hand, the investigation of the damage evolution on the butt joint specimen has shown that the material model is capable to represent the different failure modes in an engineering way. Consequently, using the material model, an ecological and economical dimensioning of assembly adhesives can be carried out.

However, further research is still needed regarding the two damage variables, as the material model along with its two damage variables is strongly motivated by an engineering point of view. In particular, the application of the volumetric damage variable needs to be reconsidered. By using a volumetric damage variable, an attempt is made to describe a discrete, volumetrically induced crack by using a delocalized damage model. However, instead of a delocalized damage model, an approach based on fracture mechanics should be used in order to be able to capture the discrete cracking in a physically correct way.

ACKNOWLEDGMENTS

Open access funding enabled and organized by Projekt DEAL.

ORCID

Aaron Schumacher https://orcid.org/0000-0001-7794-1560

REFERENCES

1. Rivlin, R. S. (1948). Large elastic deformations of isotropic materials. I. Fundamental concepts. *Philosophical Transactions of the Royal Society A: Mathematical, Physical and Engineering Sciences*, *240*, 459–490.
2. Rivlin, R. S. (1948). Large elastic deformations of isotropic materials. IV. Further developments of the general theory. *Philosophical Transactions of the Royal Society A: Mathematical, Physical and Engineering Sciences*, *241*, 379–397.
3. Holzapfel, G. A. (2000). *Nonlinear solid mechanics: A continuum approach for engineering*. Wiley.
4. Lee, E. H. (1969). Elastic-plastic deformation at finite strains. *Journal of Applied Mechanics*, *36*, 1–6.
5. Flory, P. J. (1960). Thermodynamic relations for high elastic materials. *Transactions of the Faraday Society*, *57*, 829–838.
6. Nelson, A., & Matzenmiller, A. (2017). Modelling and finite element analysis of cavitation and isochoric failure of hyperelastic adhesives. In *Constitutive models for rubber X*, CRC Press (pp. 357–363).
7. Coleman, B. D., & Noll, W. (1963). The thermodynamics of elastic materials with heat conduction and viscosity. *Archive for Rational Mechanics and Analysis*, *13*, 167–178.
8. Schumacher, A., & Matzenmiller, A. (2023). An investigation on limiting potentials for damage prediction of viscoelastic adhesives. *Proceedings in Applied Mathematics and Mechanics*, *22*, 1–6.
9. Ogden, R. W. (1972). Large deformation isotropic elasticity—On the correlation of theory and experiment for compressible rubberlike solids. *Proceedings of the Royal Society of London*, *A328*, 567–583.
10. Arruda, E. M., & Boyce, M. C. (1993). A three-dimensional constitutive model for the large stretch behaviour of rubber elastic materials. *Journal of the Mechanics and Physics of Solids*, *41*, 389–412.
11. Simo, J. C. (1987). On a fully three-dimensional finite-strain viscoelastic damage model: Formulation and computational aspects. *Computer Methods in Applied Mechanics and Engineering*, *60*, 153–173.

12. Volokh, K. Y. (2007). Hyperelasticity with softening for modeling materials failure. *Journal of the Mechanics and Physics of Solids*, *55*, 2237–2264.
13. Volokh, K. Y. (2014). On irreversibility and dissipation in hyperelasticity with softening. *Journal of Applied Mechanics*, *81*, 1–3.
14. Pijaudier-Cabot, G., & Bažant, Z. P. (1987). Nonlocal damage theory. *Journal of Engineering Mechanics*, *113*, 1512–1533.
15. Schwarzkopf, G., Hesebeck, O., & Meschut, G. (2017). Grundversuche zum material- und verbindungsverhalten. In: *Numerische Modellierung und Kennwertermittlung für das Versagensverhalten von hyperelastischen Klebverbindungen* (pp. 13–90). Abschlussbericht des Forschungsvorhabens P1086 der Forschungsvereinigung Stahlanwendungen e. V.

How to cite this article: Schumacher, A., & Matzenmiller, A. (2023). A material model for thick, rate-dependent adhesives with delocalized softening. *Proceedings in Applied Mathematics and Mechanics*, *23,* e202300032. https://doi.org/10.1002/pamm.202300032